HHS Public Access

Author manuscript

Environ Mol Mutagen. Author manuscript; available in PMC 2019 January 01.

Published in final edited form as:

Environ Mol Mutagen. 2018 January ; 59(1): 38–48. doi:10.1002/em.22138.

Thiopurine-induced mitotic catastrophe in *Rad51d*-deficient mammalian cells

Michael D. Wyatt[*,1], **Nicole M. Reilly**[1], **Shikha Patel**[1], **Preeti Rajesh**[2], **Gary P. Schools**[1], **Phillip G. Smiraldo**[3], and **Douglas L. Pittman**[*,1]

[1]Department of Drug Discovery and Biomedical Sciences, College of Pharmacy, University of South Carolina, Columbia SC 29208

[2]Department of Biotechnology, Sri Guru Granth Sahib World University, Fatehgarh Sahib, Punjab, India-140406

[3]NAMSA, Northwood, OH 43619

Abstract

Thiopurines are part of a clinical regimen used for the treatment of autoimmune disorders and childhood acute lymphoblastic leukemia. However, despite these successes, there are also unintended consequences such as therapy-induced cancer in long-term survivors. Therefore, a better understanding of cellular responses to thiopurines will lead to improved and personalized treatment strategies. RAD51D is an important component of homologous recombination (HR), and our previous work established that mammalian cells defective for RAD51D are more sensitive to the thiopurine 6-thioguanine (6TG) and have dramatically increased numbers of multinucleated cells and chromosome instability. 6TG is capable of being incorporated into telomeres, and interestingly, RAD51D contributes to telomere maintenance, although the precise function of RAD51D at the telomeres remains unclear. We sought here to investigate: 1) the activity of RAD51D at telomeres, 2) the contribution of RAD51D to protect against 6TG-induced telomere damage, and 3) the fates of *Rad51d*-deficient cells following 6TG treatment. These results demonstrate that RAD51D is required for maintaining the telomeric 3′ overhangs. As measured by γ-H2AX induction and foci formation, 6TG-induced DNA damage in *Rad51d*-proficient and *Rad51d*-deficient cells. However, the extent of γ-H2AX telomere localization following 6TG treatment was higher in *Rad51d*-deficient cells than in *Rad51d*-proficient cells. Using live-cell imaging of 6TG-treated *Rad51d*-deficient cells, two predominant forms of mitotic catastrophe were found to contribute to the formation of multinucleated cells, failed division and restitution.

[*]To whom correspondence should be addressed. Department of Drug Discovery and Biomedical Sciences, College of Pharmacy, University of South Carolina, 715 Sumter Street, Columbia SC 29208, Tel: 1 803 777 0856; fax: 1 803 777 8356. wyatt@cop.sc.edu, Tel: 1 803 777 7715; fax: 1 803 777 8356. pittman@cop.sc.edu.

Statement of Author Contributions

SP and GS performed live cell microscopy experiments and analysis. PS performed the work with primary MEFs and measurements of telomere lengths. PR developed the *Rad51d*$^{-/-}$*Mlh1*$^{-/-}$ cells. NR performed the work examining 6TG induced damage in the *Rad51d*$^{-/-}$ and *Rad51d*$^{-/-}$*Mlh1*$^{-/-}$ cells. MDW and DLP contributed to the experimental design and analysis of the data. MDW and DLP wrote the manuscript with the assistance of SP and NR. All authors provided input and final approval of the manuscript before submission.

Conflicts of Interest

All authors declare that there are no conflicts of interest.

Collectively, these findings provide a unique window into the role of the RAD51D HR protein during thiopurine induction of mitotic catastrophe.

Keywords

Telomeres; Homologous recombination; H2AX; 6-thioguanine; Mitotic catastrophe

Introduction

Thiopurines have a long history of clinical usage as immunosuppressants and in cancer chemotherapy. Combination therapy including mercaptopurine for childhood acute lymphoblastic leukemia (ALL) treatment is an amazing success story, with cure or long-term remission rates now being greater than 90%. Although the metabolism of thiopurines is well known [Krynetski & Evans 2003], surprisingly little is understood about the mechanism by which thiopurines induce DNA damage and kill cancer cells. When thiopurines are metabolized into active nucleotide forms, the predominant mechanism of action is incorporation into DNA [Karran 2006]. During replication, the thiopurine 6-thioguanine (6TG) causes base mispairing, which is then recognized by DNA mismatch repair (MMR) proteins. As part of a poorly understood process, the MMR machinery causes DNA strand breaks and invokes homologous recombination (HR) mediated repair. Inactivation or loss of MMR thus alleviates killing and chromosomal instability caused by thiopurines [Armstrong & Galloway 1997, Buermeyer et al 1999, Rajesh et al 2011].

RAD51D is one of the RAD51 family members indispensable for HR. RAD51D is now an established ovarian cancer susceptibility gene [Loveday et al 2011, Song et al 2015, Thompson et al 2013], and BRCA2-defective cancer cells are also sensitized to 6TG [Issaeva et al 2010]. Indeed, a recent phase II clinical trial, NCT01432145, explored the use of a thiopurine in BRCA2-defective tumors; based upon genetic signatures, thiopurines might be used in other HR-defective cancers. At this time, there have been no reports of the successful generation of human *knockout* cells for any of the RAD51 paralogs. In fact, vertebrate cells deficient in any of the RAD51 paralogs have only been generated in mouse embryonic fibroblasts, DT40 avian cells, and Chinese hamster ovary cells [Deans et al 2003, Hinz et al 2006, Lim & Hasty 1996, Pittman & Schimenti 2000, Takata et al 2001, Tsuzuki et al 1996]. Even though RNA interference mediated knockdowns of several of the RAD51 family members in human cancer cells have been attempted, none achieved a substantially reduced expression (e.g., RAD51 by Wyatt and coworkers [Yang et al 2008]). In all cases examined, decreased expression of the RAD51 paralogs exhibited a similar sensitivity to DNA damaging agents and chromosome instability.

Our previous work established that RAD51D-dependent HR is protective downstream of MMR following 6TG treatment [Rajesh et al 2011]. Specifically, *Rad51d*-deficient cells were extremely sensitive to 6TG, and there was a substantial increase in the frequency of chromosomal aberrations, particularly radials. There was also an increase in multinucleation and chromosomal aneuploidy in the *Rad51d*-deficient cells following 6TG treatment. The loss of MLH1 alleviated these phenotypes, demonstrating that the induced damage depends

on functional MMR. The roles of RAD51D in genomic maintenance include telomere stability [Tarsounas et al 2004]. In this regard, it is interesting to note that deoxy-thioguanine nucleotides can be incorporated into DNA by telomerase [Marathias et al 1999, Mender et al 2015, Tendian & Parker 2000]. These observations prompted our investigation into three related topics. First, we sought to better understand the specific telomeric defect associated with *Rad51d*-deficient cells. Here, it was found that RAD51D is required for maintaining the telomeric 3′ overhangs in mammalian cells. Second, we investigated telomeric DNA damage caused by 6TG. Chromosome fusions were induced by 6TG, some of which contained telomeric labeling. In *Rad51d*-deficient cells, there was increased co-localization of telomere probes with γ-H2AX foci compared to *Rad51d*-proficient cells, which further increased upon treatment with 6TG. Lastly, we investigated via live cell imaging multi-nucleation induced by 6TG treatment of *Rad51d*-deficient cells. Note that different leukemias and lymphomas are also known to have increased aneuploidy and multinucleation, and also telomere defects [Knecht et al 2009, Knecht et al 2010]. Time lapse video imaging following 6TG treatment demonstrated that *Rad51d*-deficient cells undergo primarily two forms of mitotic catastrophe, failed division and restitution, to form multinucleated cells. These findings provide a unique window into the formation of multinucleated *Rad51d*-deficient cells, and demonstrate that RAD51D provides a protective role against the telomeric DNA damage and chromosomal instability that thiopurine treatment causes.

Materials and methods

Cell lines

Mice heterozygous for a mutation in the *Mlh1* gene and mice heterozygous for null-alleles in *Rad51d* and *Trp53* were crossed to generate murine embryonic fibroblasts (MEFs) with different combinations of the three mutated genes [Rajesh et al 2011, Rajesh et al 2010, Smiraldo et al 2005]. Primary and immortalized mouse embryonic fibroblasts (MEFs) were grown in DMEM (Corning, Corning, NY USA) supplemented with 7.5% fetal bovine serum (Atlanta Biologicals, Flowery Branch, GA USA), 7.5% newborn calf serum (GE Life Sciences, Pittsburgh, PA USA), and antibiotics (GE) as previously described [Smiraldo et al 2005]. The following immortalized cell lines used for these studies were $Rad51d^{+/+}Trp53^{-/-}$ (C53), $Rad51d^{-/-}Trp53^{-/-}$ (310), and $Rad51d^{-/-}Trp53^{-/-}Mlh1^{-/-}$ (T3) cells. Note that because it was only possible to generate immortalized MEFs that were $Rad51d^{-/-}$ on a $Trp53^{-/-}$ background [Smiraldo et al 2005], all work in immortalized MEFs occurred in $Trp53^{-/-}$ cells. For simplicity, genotypes of the immortalized MEFs are referred to throughout the manuscript as *Rad51d* or *Mlh1* status.

Electrophoresis and In-gel hybridization

Experiments were performed as described [Dionne & Wellinger 1996, Hemann & Greider 1999]. Telomere lengths were estimated from radioactive signals of alkali denatured gels hybridized with the end labeled $(TTAGGG)_4$ oligonucleotide, as described [Harley et al 1990]. Relative G-strand overhang lengths were determined by the following equation, RSN/[(TLC/TLE) * RSD], where RSN is the radioactive signal from native gels hybridized with the $(CCCTAA)_4$ oligonucleotide, TLC is the estimated telomere lengths of the control

(homozygous wild-type) cells, TLE is the estimated telomere lengths, and RSD is the total radioactive signal from the denatured gels hybridized with the $(TTAGGG)_4$ oligonucleotide. Statistical significance of the experimental data was determined using SPSS® version 11.5 for Windows by ANOVA. Follow-up comparisons were performed using the Tukey HSD post hoc test.

Western blot analysis of γ-H2AX induction

Immortalized *Rad51d*$^{+/+}$, *Rad51d*$^{-/-}$, and *Rad51d*$^{-/-}$ *Mlh1*$^{-/-}$ MEFs were plated in a 6-well dish at a concentration of 6×10^4 cells per well and, after 24 h, treated with 50 or 100 nM 6TG (Sigma Aldrich, St. Louis, MO USA) for 48 and 72 h. Following treatment, cells were trypsinized and proteins extracted in 1X cell lysis buffer (20 mM Tris, 150 mM NaCl, 1 mM EDTA, 1 mM EGTA, 1 mM PMSF, 1% Triton X-100) containing protease inhibitor cocktail (Thermo Fisher, Waltham, MA USA). Thirty μg of whole-cell protein extracts were separated using a 4–20% gradient gel (Bio-Rad, Hercules, CA USA). Western blot analysis was performed using rabbit polyclonal anti-γ-H2AX (A300-081, Bethyl, Montgomery, TX USA) or rabbit monoclonal anti-GAPDH (D16H11, Cell Signaling, Danvers, MA USA). Primary incubations were followed with species specific IR Dye 800CW secondary antibody (Licor, Lincoln, NE USA), and signal detection was performed using a Licor Odyssey Sa Imaging System. Quantitative analysis of band intensity was performed using Image Studio software (LiCor, version 4.0, Lincoln NE, USA).

Immunofluorescence, telomere staining, and chromosome fusions

For the detection of γ-H2AX foci and telomere co-localization, sub-confluent cells, grown on sterile glass microscope slides or cover slips (VWR, Radnor, PA USA), were treated for the indicated times with 6TG. Following treatment, cells were fixed in 4% paraformaldehyde (Affymetrix, Santa Clara, CA USA), permeabilized with a 0.2% Triton X-100 solution, and incubated in block solution (5% dry milk in 1x PBS) at room temperature. This was followed by incubation with the anti-phospho-Histone H2AX (Ser139) mouse monoclonal antibody (1:600; Bethyl) and Oregon Green 488 goat anti-mouse IgG secondary (1:1000; Molecular Probes (Thermo Fisher), Waltham, MA USA). Telomeres were visualized with the peptide nucleic acid probe Cy3-$(CCCTAA)_3$ (PNA Bio, Thousand Oaks, CA USA) and chromatin visualized by DAPI (Sigma).

For studies using primary MEFs to detect γ-H2AX foci, cells containing ≥ 5 distinct γ-H2AX foci were defined as foci-positive, and the percentage of γ-H2AX foci at telomeres was calculated as [(number of γ-H2AX foci at telomeres)/(number of γ-H2AX foci)]* 100% for each cell. Statistical significance was determined by comparing the mean number of γ-H2AX foci at telomeres per cell for each genotype by ANOVA. Follow-up comparisons were performed using the Tukey HSD post hoc test.

For studies using immortalized MEFs and 6TG-induced damage, cells containing ≥ 10 distinct γ-H2AX foci were defined as foci-positive, and the percentage of γ-H2AX positive cells was calculated as [(number of γ-H2AX positive cells)/(total number of cells)]*100. An EvosFL fluorescence microscope (Life Technologies, Carlsbad, CA USA) under a 60X oil objective was used to detect γ-H2AX foci. Individual cells were manually scored through

depth-of-field for foci, identified based upon signal intensity above general background staining levels and present within the nucleus as assessed by DAPI staining.

Metaphase chromosome spreads were prepared as described previously [Smiraldo et al 2005]. The percent of fusions per chromosome was calculated as [(number of fusions)/(number of chromosomes)]*100 per metaphase spread. Statistical significance of the experimental data was determined by calculating a z-score. The presence of a telomere at a fusion was scored positive, and the percent telomere associated fusions was calculated as [(number of telomere positive fusions)/(number of fusions)]*100.

For detection of telomeres at chromosome fusions, an Axiovert 200 with Axiovision (Zeiss, Oberkochen, Germany) fluorescence microscope and 100X oil objective was used. For detection of γ-H2AX foci at telomeres, cells were treated as described above and the telomere $(CCCTAA)_3$ probe added after γ-H2AX antibody incubation. Individual cells were scored for co-localized foci by manual scanning through the cellular depth. Cells were scored positive when overlapping signals were observed within the nucleus. The number of γ-H2AX foci co-localized with telomere signal was counted per nuclei and grouped into three categories: 0 to 2 co-localized foci, 3 to 7 co-localized foci, or ≥8 co-localized foci. A minimum of 200 nuclei were counted for each genotype and treatment.

Live cell imaging and scoring criteria

Rad51d$^{-/-}$ cells were plated onto 35 mm glass-bottom plates (Warner Instruments, CT, USA) at a concentration of 4×10^4 cells/dish. After 24 h, cells were treated with 0, 50, or 100 nM 6TG and immediately transferred to a live-cell chamber maintained at 37°C and 5% CO_2. Grid areas selected for observation were sub-confluent, typically containing three to six individual cells in each grid, and images were captured over a minimum 72 h period at 40x magnification (DIC) (Leica Microsystems ASMDW). Nine adjacent grid areas were selected for observation, and images were captured every three minutes using a Photometrics Coolsnap HQ camera and combined into single video files using Fiji (ImageJ) software. Time in mitosis was calculated for cells from the beginning of observed rounding up until the same cell or daughter cells re-attached on the glass surface. Time in interphase was calculated as the period of time between observed mitotic events. Interphase times were not calculated for cells that did not attempt at least one mitotic division during the observation period. The mean and standard deviations were calculated using a one-tailed T-test ($p < 0.05$). Mitotic outcomes were scored as cell division, apoptosis, restitution, failed division, and mitotic arrest based upon the following criteria [Broude et al 2008]. Division events were scored as cells that completed cytokinesis and formed two distinct, mono-nuclear daughter cells. Apoptotic events were scored as cells that rounded up, formed blebbed subcellular structures and were no longer distinguishable. Restitution and failed division were scored as cellular outcomes that led to the formation of multinucleated cells during the observation period. Restitution was defined as the inability of a cell to complete cytokinesis despite the initial appearance of two daughter cells that began reattaching to the plate and subsequently fusing into a single large multinucleated cell. Failed division was defined as an event in which the cell rounded up, but there was no observable attempt at cytokinesis and the cell reattached to the glass surface. An arrest event was defined as a cell observed to

undergo one successful division but subsequently did not attempt another cell division during the experiment.

Results

RAD51D is required to maintain telomeric 3′ overhangs

Prior work from Pittman and colleagues demonstrated that *Rad51d* is essential for maintaining both chromosome and telomere stability [Smiraldo et al 2005]. However, the precise function of RAD51D at the telomere remains unresolved. Because *Rad51d* is an essential gene, a *Trp53* (p53)-deficient background was necessary to restore cell viability in order to perform the experiments as described in this manuscript in both primary and immortalized MEFs. For these experiments, we utilized two different sets of primary MEFs including $Rad51d^{+/+}$ $Trp53^{+/+}$, $Rad51d^{+/-}$ $Trp53^{+/-}$, $Rad51d^{+/+}$ $Trp53^{-/-}$, and $Rad51d^{-/-}$ $Trp53^{-/-}$ MEFs. The relative length of single-stranded, telomeric 3′ overhangs was first determined. Hybridizing a $(TTAGGG)_4$ probe on the native gels produced no signal above background (data not shown), demonstrating that the DNA in the gel was not previously nicked nor denatured. Hybridization with the $(CCCTAA)_4$ probe demonstrated 3′ overhang signals at the telomere for all genotypes (Figure 1A). Pretreatment with the single-strand-specific mung bean nuclease caused loss of signals (data not shown), demonstrating that the probe was bound to single-stranded, telomeric 3′ overhangs. Note that *Rad51d*-deficient cells have a high level of hypo- and hyperploidy [Smiraldo et al 2005], which prevented a direct comparison of signal intensity among genotypes. The DNA was next alkali denatured and hybridized with a $(TTAGGG)_4$ probe (Figure 1B). Differences of telomere lengths among samples were taken into consideration when calculating the relative length of the telomeric 3′ overhangs (Figure 1C). No significant difference in the relative length of the telomeric overhangs was observed when comparing homozygous wild-type, $Rad51d^{+/-}$ $Trp53^{+/-}$, or $Trp53^{-/-}$ cells ($p > 0.05$). However, the 1.4-fold increase in relative length of the telomeric overhangs in the $Rad51d^{-/-}$ $Trp53^{-/-}$ primary MEFs was significantly different compared to controls (homozygous wild-type vs. $Rad51d^{-/-}$ $Trp53^{-/-}$ $p \leq 0.001$, $Rad51d^{+/-}$ $Trp53^{+/-}$ vs. $Rad51d^{-/-}$ $Trp53^{-/-}$ $p = 0.001$, $Rad51d^{-/-}$ $Trp53^{-/-}$ vs. $Trp53^{-/-}$ $p \leq 0.001$).

We next determined whether spontaneous damage was evident at telomeres as measured by phosphorylated histone H2AX (ser139, γ-H2AX) in primary MEFs. When comparing the percentage of γ-H2AX foci that localized to telomeres, no significant difference was observed between homozygous wild-type and $Trp53^{-/-}$ MEFs ($p = 0.929$) (not shown). However, a 2-fold increase in the telomeric localization of γ-H2AX foci was observed in the $Rad51d^{-/-}$ $Trp53^{-/-}$ MEFs compared to the controls (Figure 1D and 1E, wild-type vs. $Rad51d^{-/-}$ $Trp53^{-/-}$ $p = 0.011$; $Trp53^{-/-}$ vs. $Rad51d^{-/-}$ $Trp53^{-/-}$ $p = 0.002$), suggesting that some telomeres are recognized as DSBs in the absence of RAD51D. Collectively, these results demonstrate that RAD51D contributes to maintaining telomeric 3′ overhangs in mammalian cells.

H2AX phosphorylation in response to 6TG treatment

Induction of γ-H2AX following 6TG treatment was assessed by Western blotting and immunofluorescence in immortalized *Rad51d*-proficient and *Rad51d*-deficient MEFs, both

in a *Trp53*-deficient background. Following treatment with 50 nM 6TG, an increase of γ-H2AX at 48 and 72 h in the *Rad51d*-proficient cells and in the *Rad51d*-deficient cells was observed (Figure 2A). At this dose and time point of 48 h, quantitation revealed that γ-H2AX was not statistically different in *Rad51d*-proficient and *Rad51d*-deficient cells (Figure 2B, grey bars, ~2.5 fold). At a 50 nM dose for 72 h, γ-H2AX was higher in *Rad51d*-proficient cells (Figure 2B, black bars, 4.5-fold compared to 2.5-fold in *Rad51d*-deficient cells). Treatment with 100 nM 6TG at 48 and 72 h induced γ-H2AX to a greater extent than that seen with 50 nM 6TG in all genotypes. No statistically significant differences were seen between *Rad51d*-proficient and *Rad51d*-deficient cells (Figure 2C). Our prior work established that in the absence of MLH1, *Rad51d*-deficient cells were less sensitive to killing and chromosomal instability caused by 6TG [Rajesh et al 2011]. In the *Rad51d*$^{-/-}$*Mlh1*$^{-/-}$ cells, there was no measurable γ-H2AX increase in the *Rad51d*$^{-/-}$*Mlh1*$^{-/-}$ cells at 50 nM 6TG at either time point (Figure 2B). At 100 nM 6TG, there was a modest induction of γ-H2AX at 100 nM 6TG that was lower compared to MLH1-proficient cells regardless of RAD51D status (Figure 2C). This is consistent with prior observations and further supports idea that the specificity of the clastogenic damage caused by 6TG in the absence of RAD51D depends on functional MMR.

Using immunofluorescence microscopy, nuclei with ten or more γ-H2AX foci after 72 h 6TG treatment were scored as positive. The untreated *Rad51d*-deficient cells had a basal level of 15% γ-H2AX foci, whereas no γ-H2AX positive *Rad51d*-proficient cells were observed (Figure 2D, white bars), indicative of the extensive genome instability associated with *Rad51d* deficiency. Following treatment with 50 nM 6TG, γ-H2AX foci positive cells increased to 42% in *Rad51d*-proficient cells, whereas in *Rad51d*-deficient cells the γ-H2AX foci positivity went from a basal level of 15% to 27% (Figure 2D, grey bars). This agreed with muted induction of H2AX by 6TG in the absence of RAD51D as observed by Western blotting in Figure 2B. At the higher dose of 100 nM 6TG, the increase in γ-H2AX foci positive cells was similar in both genotypes following treatment with 100 nM 6TG (Figure 2D, black bars). In examining the *Rad51d*$^{-/-}$*Mlh1*$^{-/-}$ cells for γ-H2AX foci, the results were entirely consistent with the observations by Western blotting for γ-H2AX in Figure 2A and 2B. Specifically, Figure 2C shows that there was no γ-H2AX foci induction above basal levels at 50 nM 6TG, whereas at the higher dose of 100 nM, a statistically significant but lessened induction of foci was observed in *Rad51d* $^{-/-}$ *Mlh1*$^{-/-}$ cells compared to the *Mlh1*$^{+/+}$ cells.

γ–H2AX and telomere co-localization in response to 6TG treatment

To determine whether γ-H2AX foci were associated with telomeres in response to 6TG, immortalized MEFs containing ≥10 γ-H2AX foci were scored after 6TG treatment (Figure 3A). Co-localization of the telomere probe with γ-H2AX foci was grouped into three categories (0–2, 3–7, and ≥8 foci/nuclei, Figure 3B). In vehicle treated, a majority (80%) of *Rad51d*-proficient cells contained between zero and two co-localized foci per nucleus (Figure 3B, left panel, white portion of bar). In contrast, the majority (>60%) of vehicle-treated *Rad51d*-deficient cells contained three or more co-localized foci per nucleus (Figure 3B, middle panel, grey portion) indicative of an elevated basal level of DNA damage in the absence of RAD51D. In response to 50 nM 6TG treatment, there was an induction of co-

localized foci per nucleus in *Rad51d*-proficient cells (Figure 3B, left panel). In *Rad51d*-deficient cells, 50 nM 6TG treatment caused a large increase in the number of cells with 8+ co-localized foci (Figure 3B, middle panel, black portion). The higher dose of 100 nM induced an equivalent co-localization in *Rad51d*-proficient and *Rad51d*-deficient cells (Figure 3B, left versus middle panel). These data demonstrate that 6TG induced DNA damage as visualized by γ-H2AX at telomeres in a dose-dependent manner, and at least at the lower dose of 6TG, there is more telomeric damage in the absence of RAD51D. Figure 3B (right panel) also shows that γ-H2AX localization at telomeres is reduced in the absence of MLH1, which is consistent with prior work showing that MMR recognition of 6TG damage promotes clastogenic events.

Previously, we reported a striking induction of radial chromosomes in *Rad51d*-deficient cells following 6TG treatment [Rajesh et al 2011]. To determine whether chromosome fusions were associated with telomere ends, telomere associated fusions were examined in metaphase spreads. As expected, no fusions were detected in vehicle treated *Rad51d*-proficient cells (Table 1; n=1005 scored). After treatment with 50 or 100 nM 6TG, the number of fusions observed in *Rad51d*-proficient cells was detectable but, as expected, remained low, 0.4 and 0.8%, respectively (Figure 4, white bars). Too few fusions were observed to clearly determine telomere association (Table 1). In the vehicle-treated *Rad51d*-deficient cells, a basal level of 1.1% chromosome fusions was detected, which increased to 2.7% and 6.9% following treatment with 50 and 100 nM 6TG, respectively (Figure 4, grey bars, $p<0.05$). In vehicle-treated *Rad51d*-deficient cells, telomere-associated fusions were detectable and do appear to increase following 6TG treatment, but the level of fusions regardless of telomere association was too few to make any statistically meaningful conclusions (Table 1). Lastly, a basal level of 0.6% chromosome fusions was detected in the $Rad51d^{-/-}Mlh1^{-/-}$ cells, which increased by a statistically insignificant amount to 0.9% and 1.6% following treatment with 50 and 100 nM 6TG, respectively (Figure 4, black bars). The data showing that 6TG-induced fusions was reduced in *Mlh1*-deficient cells agreed with prior data from us and others that the cytogenetic damage caused by 6TG is dependent at least in part on functional MMR [Armstrong & Galloway 1997, Rajesh et al 2011].

6-Thioguanine induces mitotic catastrophe in Rad51d-deficient cells

Our prior work demonstrated that treatment with 100 nM 6TG induced aneuploidy and multinucleation in *Rad51d*-deficient cells [Rajesh et al 2011]. Here, the induction of multinucleated cells was verified following treatment with a lower dose of 50 nM 6TG (Supplemental Figure 1). Note also we investigated whether there was an unequal distribution of telomeric DNA in the multinucleated cells because of such observations in a prior report [Knecht et al 2009]. However, we show in Supplemental Figure 2 that the multinucleated cells contained an equal distribution of telomeric DNA in this experimental system.

To investigate the origins of the multinucleated phenotype after 6TG exposure, time lapse video imaging was used to monitor mitotic events over the course of at least 72 h of drug exposure. *Rad51d*-deficient cells treated with 50 nM 6TG had an increased time in interphase by 16 h (from 24 to 40 h) compared with untreated cells (Figure 5A, $p=3.31 \times$

10^{-6}). *Rad51d*-deficient MEFs treated with 100 nM 6TG showed an increased time in interphase by 9 h (from 24 to 33 h) compared to untreated cells (Figure 5A, $p=2.98 \times 10^{-7}$). *Rad51d*-deficient cells treated with 50 nM 6TG also spent twice as much time completing mitosis compared to untreated cells (p=0.035), whereas cells treated with 100 nM 6TG spent a similar time in mitosis as the untreated cells (p= 0.237) (Figure 5B). The number of apoptotic, restitution, and failed division events were substantially increased in *Rad51d*-deficient cells treated with 50 nM 6TG (Figure 5C, grey bars), whereas a greater percentage of cells treated with 100 nM 6TG (black bars) had an increased number of arrested cells. These observations at the higher dose are consistent with the dose-dependent G2 arrest previously observed [Rajesh et al 2011]. An example of a failed division following treatment with 50 nM 6TG is shown in Figure 5D and as supplementary video 1. In the center of the field, a cell is observed to round up at the start of mitosis (time-stamp 69:39) and attempt to divide for greater than 2 hours, before re-attaching to the glass surface as a single multinucleated cell (time-stamp 73:48). An example of a restitution event observed following treatment with 50 nM 6TG is shown in Figure 5E and as supplementary video 2. The cell is observed to round up (time-stamp 33:09) and divide into what appears to be three daughter cells (35:39). The daughter cells fail to complete cytokinesis, and fuse into a single multinucleated cell (37:06).

Discussion

Thiopurines induce a G2 arrest, which presumably prevents cells with damaged DNA from entering what would otherwise become an abnormal mitosis [Armstrong & Galloway 1997, Buermeyer et al 1999, Rajesh et al 2011]. However, co-treatment with caffeine or UCN-01 to block ATM/ATR signaling can override the G2 arrest, from which cells subsequently enter tetraploid G1 arrest [Yan et al 2004]. In *Rad51d*-deficient cells, the G2 arrest caused by 6TG was heightened but transient; by 72 h, both *Rad51d*-deficient and *Rad51d*-proficient cells progressed into mitosis, as demonstrated by flow cytometry and phospho-histone H3 staining [Rajesh et al 2011]. One implication is that release from this G2 checkpoint does not require the resolution/completion of HR, and as such might help explain how cancer cells achieve aneuploidy. 6TG treatment induced aneuploidy and multinucleated cells [Rajesh et al 2011]. Similar to this *Rad51d*-deficient cellular phenotype, different leukemia and lymphomas are known to have increased aneuploidy and multinucleation. One notable example is Reed-Sternberg (RS) cells associated with the pathology of Hodgkin's lymphoma [Mauch 2006]. The data presented here demonstrates that multinucleation following 6TG treatment occurs via mitotic catastrophe in two ways: failed division and restitution. In this system, mitotic catastrophe resulted in multinucleated cells that do not undergo apoptosis over the duration of the observations here. When treated with the 50 nM 6TG dose, a larger percentage of multinucleated *Rad51d*-deficient cells undergo mitotic catastrophe, which was not observed in cells at the 100 nM dose presumably because of the heightened arrest. These results suggest that a percentage of cells progress into mitosis at the lower dose of 6TG. In fact, multinucleation and mitotic catastrophe is proposed to be a favored cell death mechanism after cell cycle arrest [Castedo et al 2004, Fragkos & Beard 2011].

Phosphorylation of Serine-139 on H2AX was measured as a marker of DNA damage, and 6TG induced γ-H2AX as measured by Western blotting and immunofluorescence in both *Rad51d*-deficient and *Rad51d*-proficient cells. It was interesting to note that, as detected by Western blotting and immunofluorescence, γ-H2AX induction seemed muted in the *Rad51d*-deficient cells at the lower dose of 50 nM. It is tempting to speculate that the absence of RAD51D disrupts not just HR repair but also associated DNA damage signaling. In fact, a role for the paralog RAD51C in checkpoint signaling was demonstrated [Badie et al 2009]. However, note that γ-H2AX induction is a highly dynamic process intertwined with yet to be clarified connections with the induction of apoptosis and a broader epigenetic reprogramming in cancer [Cook et al 2009, Liu et al 2016, Lu et al 2006, Monteiro et al 2014, Xiao et al 2009].

RAD51D, a protein required for HR, was demonstrated previously to have a role in telomere protection [Tarsounas et al 2004]. Loss of RAD51D conferred extensive chromosome instability, increased chromosome fusions, and accelerated telomere attrition [Smiraldo et al 2005, Tarsounas et al 2004]. To further examine the role of RAD51D at telomeres, we analyzed the length of the 3′ telomeric overhanging tail in *Rad51d*-deficient MEFs. *Rad51d*-deficient cells had an approximately 40 percent increase in overhang signal intensity. These data demonstrate that loss of RAD51D affects the length of the 3′ telomeric overhang, and suggest that RAD51D is required for the regulation of telomere termini. Telomere dysfunction is known to activate DNA damage responses, and loss of murine exonuclease 1 (Exo1) alleviated deleterious cellular responses in telomere dysfunctional mice [Schaetzlein et al 2007]. This implies that damage disrupting the normal telomere protective mechanisms can expose chromosome ends to exonucleolytic processing that can promote chromosome fusions. Exo1 deletion also conferred cellular resistance to killing by 6TG [Schaetzlein et al 2007], which implicates telomeric damage as a mechanism of action for 6TG. Because mammalian telomeres contain a G_3 repeat in its canonical sequence, 6TG (as the deoxynucleoside triphosphate) can become incorporated into telomeric DNA by telomerase [Marathias et al 1999, Tendian & Parker 2000]. It was more recently reported that the deoxynucleoside of 6TG can directly damage telomeric DNA, and that hTERT positive cells are sensitized to this treatment [Mender et al 2015]. We measured the distribution of telomeres in the multinucleated *Rad51d*-deficient cells because prior reports have shown structural telomeric defects and unequal distribution in multinucleated Reed-Sternberg cells [Knecht et al 2009, Knecht et al 2010]. However, no unequal telomere distribution was observed in the *Rad51d*-deficient MEFs after 6TG treatment. Collectively, this work contributes to the understanding of 6TG-induced telomere damage and the negative consequences for chromosomal instability in the absence of RAD51D-dependent processes at telomeres.

RAD51D is a RAD51 family member broadly appreciated to be indispensable for HR; yet, the specialized functions of the individual protein products have evaded full elucidation. Components of HR are recruited to stalled replication forks and inter-strand crosslinks (ICLs), as well as DNA double strand breaks (DSBs). Recently, a dominant RAD51 mutation in a patient with Fanconi anemia-like phenotypes was characterized and uncovered a role for RAD51 in ICL repair independent of HR [Wang et al 2015], suggesting there is much more to learn about these highly related yet potentially separable processes. Human

variant alleles of the RAD51 paralogs confer cancer susceptibility, for example RAD51B mutations are associated with breast cancer [Golmard et al 2013, Pelttari et al 2016], RAD51C mutations are associated with breast and ovarian cancer, and RAD51D mutations are associated with ovarian cancer [Coulet et al 2013, Meindl et al 2010, Song et al 2015, Vaz et al 2010]. There are many more mutations of unknown significance in these paralogs. Our results suggest that clinical variability in how patients respond to thiopurine treatment, as well as their potential risk for a future, therapy-related secondary dysplasia might include the status of RAD51D-dependent processing of telomeres.

Supplementary Material

Refer to Web version on PubMed Central for supplementary material.

Acknowledgments

Grant Support: This research was supported in part by a grant from the NIH to the Center for Colon Cancer Research at USC (P20 RR17698), from the American Cancer Society to DLP (RSG-03-158-01-GMC), a Helen and Harold McMaster Endowment to DLP, an SC Honors College Science Undergraduate Research Fellowship to SP, and the National Institute of General Medical Sciences of the National Institutes of Health Award Number R15 GM110615. The content is solely the responsibility of the authors and does not necessarily represent the official views of the National Institutes of Health.

We thank Dr. Deanna Smith, Mr. Timothy Hines, and Ms. Latarsha Porcher for assistance with fluorescence microscopy.

Grant Sponsors

This research was supported in part by a grant from the NIH to the Center for Colon Cancer Research at USC (P30 GM103336), from the American Cancer Society to DLP (RSG-03-158-01-GMC), a Helen and Harold McMaster Endowment to DLP, an SC Honors College Science Undergraduate Research Fellowship to SP, and the National Institute of General Medical Sciences of the National Institutes of Health Award Number R15 GM110615. The content is solely the responsibility of the authors and does not necessarily represent the official views of the National Institutes of Health.

References

Armstrong MJ, Galloway SM. Mismatch repair provokes chromosome aberrations in hamster cells treated with methylating agents or 6-thioguanine, but not with ethylating agents. Mutation Research. 1997; 373:167–178. [PubMed: 9042397]

Badie S, Liao C, Thanasoula M, Barber P, Hill MA, Tarsounas M. Rad51c facilitates checkpoint signaling by promoting chk2 phosphorylation. The Journal of cell biology. 2009; 185:587–600. [PubMed: 19451272]

Broude, EV., Loncarek, J., Wada, I., Cole, K., Hanko, C., Roninson, IB., Swift, M. Mitotic catastrophe in cancer therapy. In: Roninson, IB.Brown, JM., Bredesen, DE., editors. Beyond apoptosis: Cellular outcomes of cancer therapy. CRC Press; 2008. p. 307-320.

Buermeyer AB, Wilson-Van Patten C, Baker SM, Liskay RM. The human mlh1 cdna complements DNA mismatch repair defects in mlh1-deficient mouse embryonic fibroblasts. Cancer research. 1999; 59:538–541. [PubMed: 9973196]

Castedo M, Perfettini JL, Roumier T, Andreau K, Medema R, Kroemer G. Cell death by mitotic catastrophe: A molecular definition. Oncogene. 2004; 23:2825–2837. [PubMed: 15077146]

Cook PJ, Ju BG, Telese F, Wang X, Glass CK, Rosenfeld MG. Tyrosine dephosphorylation of h2ax modulates apoptosis and survival decisions. Nature. 2009; 458:591–596. [PubMed: 19234442]

Coulet F, Fajac A, Colas C, Eyries M, Dion-Miniere A, Rouzier R, Uzan S, Lefranc JP, Carbonnel M, Cornelis F, et al. Germline rad51c mutations in ovarian cancer susceptibility. Clinical genetics. 2013; 83:332–336. [PubMed: 22725699]

Deans B, Griffin CS, O'Regan P, Jasin M, Thacker J. Homologous recombination deficiency leads to profound genetic instability in cells derived from xrcc2-knockout mice. Cancer research. 2003; 63:8181–8187. [PubMed: 14678973]

Dionne I, Wellinger RJ. Cell cycle-regulated generation of single-stranded g-rich DNA in the absence of telomerase. Proceedings of the National Academy of Sciences of the United States of America. 1996; 93:13902–13907. [PubMed: 8943033]

Fragkos M, Beard P. Mitotic catastrophe occurs in the absence of apoptosis in p53-null cells with a defective g1 checkpoint. PloS one. 2011; 6:e22946. [PubMed: 21853057]

Golmard L, Caux-Moncoutier V, Davy G, Al Ageeli E, Poirot B, Tirapo C, Michaux D, Barbaroux C, d'Enghien CD, Nicolas A, et al. Germline mutation in the rad51b gene confers predisposition to breast cancer. BMC cancer. 2013; 13:484. [PubMed: 24139550]

Harley CB, Futcher AB, Greider CW. Telomeres shorten during ageing of human fibroblasts. Nature. 1990; 345:458–460. [PubMed: 2342578]

Hemann MT, Greider CW. G-strand overhangs on telomeres in telomerase-deficient mouse cells. Nucleic acids research. 1999; 27:3964–3969. [PubMed: 10497259]

Hinz JM, Tebbs RS, Wilson PF, Nham PB, Salazar EP, Nagasawa H, Urbin SS, Bedford JS, Thompson LH. Repression of mutagenesis by rad51d-mediated homologous recombination. Nucleic acids research. 2006; 34:1358–1368. [PubMed: 16522646]

Issaeva N, Thomas HD, Djurenovic T, Jaspers JE, Stoimenov I, Kyle S, Pedley N, Gottipati P, Zur R, Sleeth K, et al. 6-thioguanine selectively kills brca2-defective tumors and overcomes parp inhibitor resistance. Cancer research. 2010; 70:6268–6276. [PubMed: 20631063]

Karran P. Thiopurines, DNA damage, DNA repair and therapy-related cancer. Br Med Bull. 2006; 79–80:153–170.

Knecht H, Sawan B, Lichtensztejn D, Lemieux B, Wellinger RJ, Mai S. The 3d nuclear organization of telomeres marks the transition from hodgkin to reed-sternberg cells. Leukemia. 2009; 23:565–573. [PubMed: 19039323]

Knecht H, Sawan B, Lichtensztejn Z, Lichtensztejn D, Mai S. 3d telomere fish defines lmp1-expressing reed-sternberg cells as end-stage cells with telomere-poor 'ghost' nuclei and very short telomeres. Lab Invest. 2010; 90:611–619. [PubMed: 20142802]

Krynetski E, Evans WE. Drug methylation in cancer therapy: Lessons from the tpmt polymorphism. Oncogene. 2003; 22:7403–7413. [PubMed: 14576848]

Lim DS, Hasty P. A mutation in mouse rad51 results in an early embryonic lethal that is suppressed by a mutation in p53. Molecular and cellular biology. 1996; 16:7133–7143. [PubMed: 8943369]

Liu F, Wang L, Perna F, Nimer SD. Beyond transcription factors: How oncogenic signalling reshapes the epigenetic landscape. Nature reviews Cancer. 2016; 16:359–372. [PubMed: 27220480]

Loveday C, Turnbull C, Ramsay E, Hughes D, Ruark E, Frankum JR, Bowden G, Kalmyrzaev B, Warren-Perry M, Snape K, et al. Germline mutations in rad51d confer susceptibility to ovarian cancer. Nat Genet. 2011; 43:879–882. [PubMed: 21822267]

Lu C, Zhu F, Cho YY, Tang F, Zykova T, Ma WY, Bode AM, Dong Z. Cell apoptosis: Requirement of h2ax in DNA ladder formation, but not for the activation of caspase-3. Molecular cell. 2006; 23:121–132. [PubMed: 16818236]

Marathias VM, Sawicki MJ, Bolton PH. 6-thioguanine alters the structure and stability of duplex DNA and inhibits quadruplex DNA formation. Nucleic acids research. 1999; 27:2860–2867. [PubMed: 10390526]

Mauch, PM., Weiss, L., Armitage, JO. Hodgkin disease. In: Kufe, DW.Bast, RC.Hait, WN.Hong, WK.Pollock, RE.Weichselbaum, RR.Holland, JF., Frei, E., editors. Cancer medicine. Hamilton, Ontario Canada: BC Decker; 2006. p. 1802-1824.

Meindl A, Hellebrand H, Wiek C, Erven V, Wappenschmidt B, Niederacher D, Freund M, Lichtner P, Hartmann L, Schaal H, et al. Germline mutations in breast and ovarian cancer pedigrees establish rad51c as a human cancer susceptibility gene. Nat Genet. 2010; 42:410–414. [PubMed: 20400964]

Mender I, Gryaznov S, Dikmen ZG, Wright WE, Shay JW. Induction of telomere dysfunction mediated by the telomerase substrate precursor 6-thio-2′-deoxyguanosine. Cancer discovery. 2015; 5:82–95. [PubMed: 25516420]

Monteiro FL, Baptista T, Amado F, Vitorino R, Jeronimo C, Helguero LA. Expression and functionality of histone h2a variants in cancer. Oncotarget. 2014; 5:3428–3443. [PubMed: 25003966]

Pelttari LM, Khan S, Vuorela M, Kiiski JI, Vilske S, Nevanlinna V, Ranta S, Schleutker J, Winqvist R, Kallioniemi A, et al. Rad51b in familial breast cancer. PloS one. 2016; 11:e0153788. [PubMed: 27149063]

Pittman DL, Schimenti JC. Midgestation lethality in mice deficient for the RecA-related gene, rad51d/rad51l3. Genesis. 2000; 26:167–173. [PubMed: 10705376]

Rajesh P, Litvinchuk A, Pittman DL, Wyatt MD. The homologous recombination protein rad51d mediates the processing of 6-thioguanine lesions downstream of mismatch repair. Mol Cancer Res. 2011; 9:206–214. [PubMed: 21205838]

Rajesh P, Rajesh C, Wyatt MD, Pittman DL. Rad51d protects against mlh1-dependent cytotoxic responses to O(6)-methylguanine. DNA repair. 2010; 9:458–467. [PubMed: 20133210]

Schaetzlein S, Kodandaramireddy NR, Ju Z, Lechel A, Stepczynska A, Lilli DR, Clark AB, Rudolph C, Kuhnel F, Wei K, et al. Exonuclease-1 deletion impairs DNA damage signaling and prolongs lifespan of telomere-dysfunctional mice. Cell. 2007; 130:863–877. [PubMed: 17803909]

Smiraldo PG, Gruver AM, Osborn JC, Pittman DL. Extensive chromosomal instability in rad51d-deficient mouse cells. Cancer research. 2005; 65:2089–2096. [PubMed: 15781618]

Song H, Dicks E, Ramus SJ, Tyrer JP, Intermaggio MP, Hayward J, Edlund CK, Conti D, Harrington P, Fraser L, et al. Contribution of germline mutations in the rad51b, rad51c, and rad51d genes to ovarian cancer in the population. Journal of clinical oncology: official journal of the American Society of Clinical Oncology. 2015; 33:2901–2907. [PubMed: 26261251]

Takata M, Sasaki MS, Tachiiri S, Fukushima T, Sonoda E, Schild D, Thompson LH, Takeda S. Chromosome instability and defective recombinational repair in knockout mutants of the five rad51 paralogs. Molecular and cellular biology. 2001; 21:2858–2866. [PubMed: 11283264]

Tarsounas M, Munoz P, Claas A, Smiraldo PG, Pittman DL, Blasco MA, West SC. Telomere maintenance requires the rad51d recombination/repair protein. Cell. 2004; 117:337–347. [PubMed: 15109494]

Tendian SW, Parker WB. Interaction of deoxyguanosine nucleotide analogs with human telomerase. Mol Pharmacol. 2000; 57:695–699. [PubMed: 10727514]

Thompson ER, Rowley SM, Sawyer S, kConfab, Eccles DM, Trainer AH, Mitchell G, James PA, Campbell IG. Analysis of rad51d in ovarian cancer patients and families with a history of ovarian or breast cancer. PloS one. 2013; 8:e54772. [PubMed: 23372765]

Tsuzuki T, Fujii Y, Sakumi K, Tominaga Y, Nakao K, Sekiguchi M, Matsushiro A, Yoshimura Y, Morita T. Targeted disruption of the rad51 gene leads to lethality in embryonic mice. Proceedings of the National Academy of Sciences of the United States of America. 1996; 93:6236–6240. [PubMed: 8692798]

Vaz F, Hanenberg H, Schuster B, Barker K, Wiek C, Erven V, Neveling K, Endt D, Kesterton I, Autore F, et al. Mutation of the rad51c gene in a fanconi anemia-like disorder. Nat Genet. 2010; 42:406–409. [PubMed: 20400963]

Wang AT, Kim T, Wagner JE, Conti BA, Lach FP, Huang AL, Molina H, Sanborn EM, Zierhut H, Cornes BK, et al. A dominant mutation in human rad51 reveals its function in DNA interstrand crosslink repair independent of homologous recombination. Molecular cell. 2015; 59:478–490. [PubMed: 26253028]

Xiao A, Li H, Shechter D, Ahn SH, Fabrizio LA, Erdjument-Bromage H, Ishibe-Murakami S, Wang B, Tempst P, Hofmann K, et al. Wstf regulates the h2a.X DNA damage response via a novel tyrosine kinase activity. Nature. 2009; 457:57–62. [PubMed: 19092802]

Yan T, Desai AB, Jacobberger JW, Sramkoski RM, Loh T, Kinsella TJ. Chk1 and chk2 are differentially involved in mismatch repair-mediated 6-thioguanine-induced cell cycle checkpoint responses. Molecular cancer therapeutics. 2004; 3:1147–1157. [PubMed: 15367709]

Yang Z, Waldman AS, Wyatt MD. DNA damage and homologous recombination signaling induced by thymidylate deprivation. Biochemical pharmacology. 2008; 76:987–996. [PubMed: 18773878]

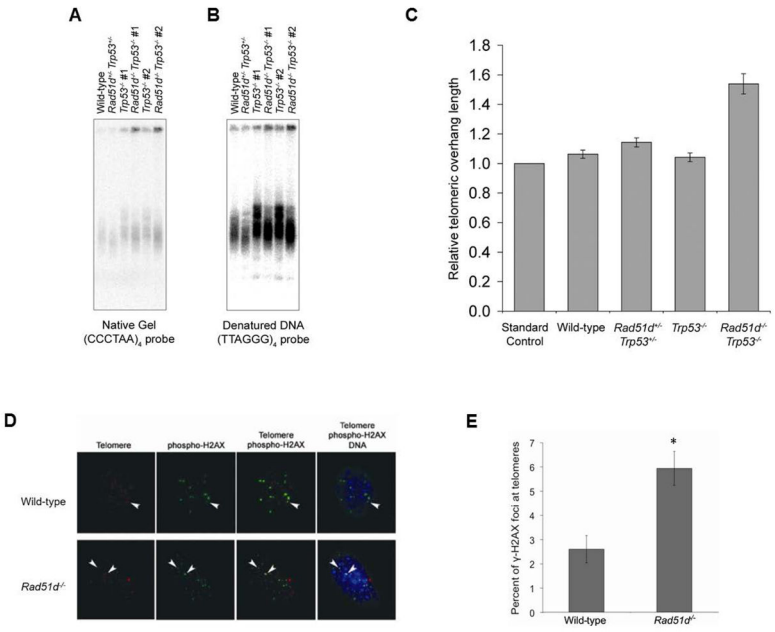

Figure 1.

Comparison of relative telomeric 3′ overhang lengths in primary MEFs. **(A)** Radioactively labeled oligonucleotide in-gel hybridizations to *Mbo*I digested genomic DNA isolated from primary MEFs. A native gel was first hybridized with the $(CCCTAA)_4$ probe, and **(B)** the same gel was alkali denatured and hybridized with the $(TTAGGG)_4$ probe. **(C)** Relative G-strand overhang lengths were determined using the following equation: $RS_N/[(TL_C/TL_E) * RS_D]$, where RS_N is the radioactive signal from native gels hybridized with the $(CCCTAA)_4$ oligonucleotide, TL_C is the estimated telomere lengths of the control (homozygous wild-type) cells, TL_E is the estimated telomere lengths of the primary wild-type, *Rad51d*$^{+/-}$ *Trp53*$^{+/-}$, *Trp53*$^{-/-}$, *or Rad51d*$^{-/-}$ *Trp53*$^{-/-}$ cells, and RS_D is the total radioactive signal from the denatured gels hybridized with the $(TTAGGG)_4$ oligonucleotide. Telomere lengths were estimated as described [Harley et al 1990]. Error bars are the SEM from at least three independent experiments. (**D)** Localization of γ-H2AX foci at telomeres in primary MEFs. Telomeric DNA was identified by the peptide nucleic acid (PNA) probe (red), γ-H2AX was immunolabeled by indirect immunofluorescence (green), and DNA stained with DAPI (blue). White arrowheads demonstrate the localization of γ-H2AX foci at telomeres. (**E**) Percentage of γ-H2AX foci at telomeres in primary wild-type MEFs (n = 58 nuclei scored) and primary *Rad51d* $^{-/-}$ MEFs (n = 59 nuclei scored). Statistical significance was calculated by ANOVA; *indicated p=0.011.

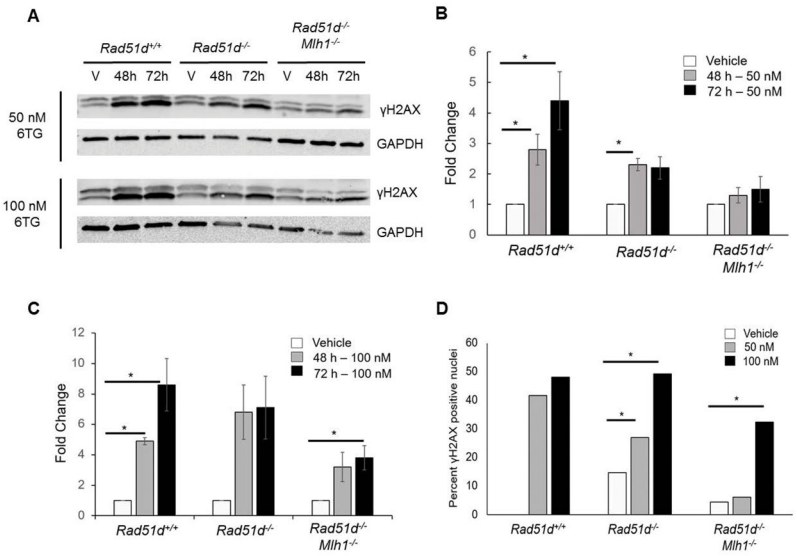

Figure 2.

Induction of γ-H2AX following treatment with 6TG. **(A)** The γ-H2AX signal (lower band) was determined by Western blot analysis after 6TG treatment for 48 and 72 h at the doses indicated in *Rad51d*$^{+/+}$ (lanes 1 – 3) and *Rad51d*$^{-/-}$ (lanes 4 – 6) and *Rad51d*$^{-/-}$*Mlh1*$^{-/-}$ MEFs (lanes 7 – 9). **(B & C)** Quantification of γ-H2AX band intensities from untreated cells (☐), or cells treated for 48 h (■) or 72 h (■) that were normalized to GAPDH (*$p<0.05$) after 50 nM (**B**) or 100 nM **(C)** 6TG treatment. **(D)** Quantitation of cellular γ-H2AX foci from untreated cells (☐), or cells treated with 50 (■) or 100 nM (■) 6TG. Nuclei with ten or more γ-H2AX foci were scored as positive, and at least 100 nuclei were counted for each sample.

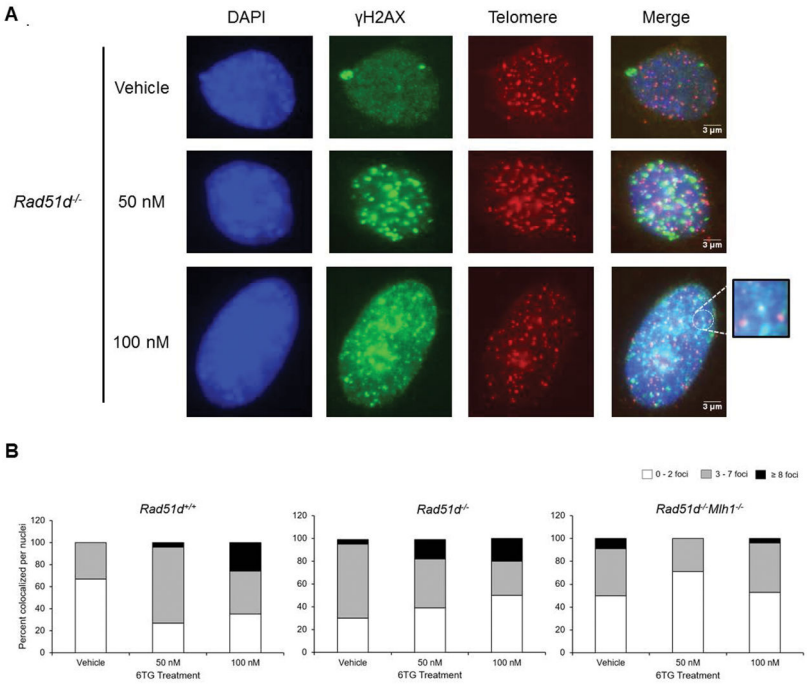

Figure 3.

(A). Localization of γ-H2AX foci co-localized with telomere signal at telomeres in immortalized MEFs after treatment with vehicle alone, 50 nM, or 100 nM 6TG. The three categories are 0 to 2 co-localized foci (□), 3 to 7 co-localized foci (■), or ≥8 co-localized foci (■) per nuclei. **(B).** Representative images of *Rad51d*$^{-/-}$ cells mock treated or treated with 50 or 100 nM 6TG. Blue panels are DAPI stained nuclei. Green panels are stained with anti- γ-H2AX antibody. Red panels are stained with the telomere probe. Merge is the overlay of each panel.

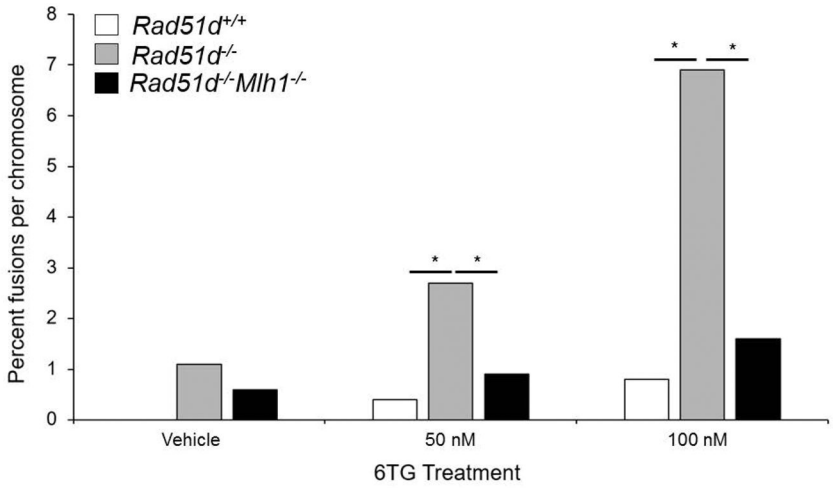

Figure 4.

6TG induced chromosome fusions in *Rad51d*-deficient immortalized MEFs. After treatment for 72 hours, chromosomes were stained with DAPI. The number of chromosome fusions was scored as a percent of the total number of chromosomes in vehicle, 50 nM, or 100 nM 6TG-treated $Rad51d^{+/+}$ (□), and $Rad51d^{-/-}$ (■) and $Rad51d^{-/-}Mlh1^{-/-}$ MEFs (■) Statistical significance was determined by calculating a z-score; *indicates $p<0.05$.

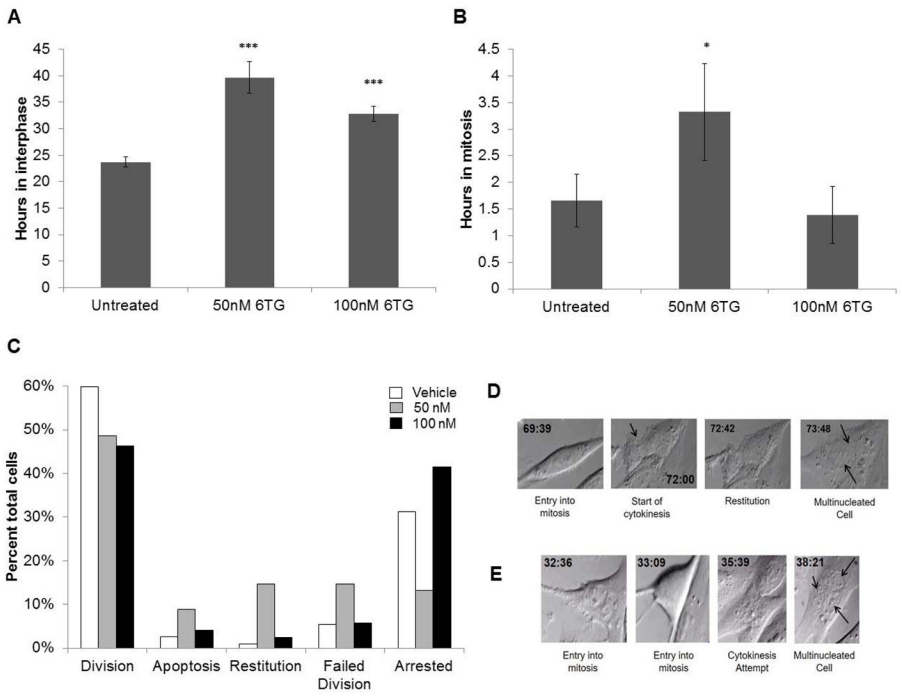

Figure 5.

Morphological analysis of *Rad51d*-deficient MEFs following 6TG treatment. The average time of immortalized *Rad51d*$^{-/-}$ MEFs spent in **(A)** interphase and (**B)** mitosis is shown. Statistical significance was determined by one-tailed T test; error bars indicate the standard deviation; *** indicates $p<0.001$. * indicates $p<0.05$. **(C)** Cellular outcomes of nine grids from three independent experiments after no treatment, treatment with 50 nM or 100 nM 6TG scored as division, apoptosis, restitution, failed division, and arrest. The total number of cells scored were 112 for untreated (☐), 68 for cells treated with 50 nM 6TG (■) and 123 for cells treated with 100 nM 6TG (■). **(D & E)** Representative still images show multi-nucleation events as a result of restitution (D) or failed division (E). The arrow in the second panel of (D) indicates the beginning of cytokinesis, and the arrows in the fourth panel indicate each nucleus within a single cell. The arrows in the fourth panel of (E) indicate each nucleus within a single cell.

Table 1

Cytological analysis of MEFs treated with 6TG

(A) Vehicle treated MEFs			
Genotype	***Rad51d*$^{+/+}$**	***Rad51d*$^{-/-}$**	***Rad51d*$^{-/-}$*Mlh1*$^{-/-}$**
Number of chromosomes	1005	462	980
End-to-end fusions[a]	0(0)	0.01(5)	0.01(6)
−TTAGGG[b]	0(0)	0.60(3)	0.33(2)
+TTAGGG[b]	0(0)	0.40(2)	0.67(4)
(B) 50 nM 6TG treated MEFs			
Genotype	*Rad51d*$^{+/+}$	*Rad51d*$^{-/-}$	*Rad51d*$^{-/-}$*Mlh1*$^{-/-}$
Number of chromosomes	552	587	572
End-to-end fusions[a]	0(2)	0.03(16)	0.01(5)
−TTAGGG[b]	1(2)	0.75(12)	0(0)
+TTAGGG[b]	0(0)	0.25(4)	1(5)
(C) 100 nM 6TG treated MEFs			
Genotype	*Rad51d*$^{+/+}$	*Rad51d*$^{-/-}$	*Rad51d*$^{-/-}$*Mlh1*$^{-/-}$
Number of chromosomes	522	463	632
End-to-end fusions[a]	0.01(4)	0.07(32)	0.02(10)
−TTAGGG[b]	0.75(3)	0.66(21)	0(0)
+TTAGGG[b]	0.25(1)	0.34(11)	1(10)

[a]Frequency of end-to-end fusions represented as the percentage of the total number of chromosomes scored for that sample. The total number is shown in parentheses.

[b]+TTAGGG and −TTAGGG refer to the presence or absence of telomeric repeats at the fusion point.